Electron-electron interactions and charging effects in graphene quantum dots

B. Wunsch,[1,2] T. Stauber,[2,3] and F. Guinea[2]

[1]*Departamento de Física de Materiales, Facultad de Ciencias Físicas, Universidad Complutense de Madrid, E-28040 Madrid, Spain*

[2]*Instituto de Ciencia de Materiales de Madrid, CSIC, Cantoblanco, E-28049 Madrid, Spain*

[3]*Center of Physics and Departamento de Física, Universidade do Minho, P-4710-057 Braga, Portugal*

(Received 9 October 2007; published 15 January 2008)

We analyze charging effects in graphene quantum dots. Using a simple model, we show that when the Fermi level is far from the neutrality point, charging effects lead to a shift in the electrostatic potential and the dot shows standard Coulomb blockade features. Near the neutrality point, surface states are partially occupied and the Coulomb interaction leads to a strongly correlated ground state, which can be approximated by either a Wigner crystal or a Laughlin-like wave function. The existence of strong correlations modifies the transport properties, which show nonequilibrium effects, similar to those predicted for tunneling into other strongly correlated systems.

DOI: 10.1103/PhysRevB.77.035316 PACS number(s): 73.63.Kv, 73.23.Hk, 73.43.Lp

I. INTRODUCTION

Graphene has attracted a great deal of attention because of its novel fundamental properties and its potential applications.[1] The interest on graphene devices has motivated recent research on the transport properties of small devices.[2–5] Features such as charging effects and quantum confinement are of crucial importance for their understanding.[6,7] The confinement of electrons and the observation of Coulomb blockade effects have already been demonstrated experimentally.[1,8] Note that the confinement of electrons in graphene is not trivial due to *Klein's paradox*,[9] which makes potential barriers transparent for normally incident quasiparticles. Electrons in graphene can be confined, however, by exploiting the angular dependence of scattering at a barrier.[10]

For graphene layers, electron-electron interaction is usually neglected, including works on localization[11] even though disorder enhances the effect of interaction.[12] The reasoning for this is to assume a "normal" ground state at zero doping—characterized by a semimetal. Because the kinetic and interaction energies equally scale with the carrier density, the interaction does not become important at finite doping either. It is thus well agreed on that at finite doping electron-electron interaction can be treated within the random-phase approximation (RPA).[13,14] Nevertheless, at the Dirac point, RPA seems to fail, leading to a novel plasmon mode in graphene.[15] Also in a quantum dot, we find that electron-electron interaction has to be treated differently for doping regimes close to and away from the Dirac point.

The main part of this work is the prediction and characterization of strongly correlated few-electron states in graphene quantum dots. Similar studies have been performed previously for semiconducting quantum dots.[16–19] In order to obtain strongly correlated ground states, the Coulomb interaction has to dominate over the other energy scale, namely, the shell structure of the single particle spectrum determined by the confinement. This is typically achieved either by using strong magnetic fields,[17,18] so that the single particle levels form highly degenerate Landau levels, or by using rather weak confinement.[16] Interestingly, strongly correlated states naturally arise already in small graphene quantum dots even without magnetic field. The reason for that is the appearance of a highly degenerate zero energy band of surface states, which is strongly affected by Coulomb interaction. Close to half filling, these states are occupied by few electrons, which are strongly correlated and can be approximated by a Laughlin-like wave function or alternatively by a quasi-one-dimensional Wigner crystal.

The paper is organized as follows. In Sec. II, we present a simple model that allows us to describe qualitatively the charging of a graphene dot. In Sec. III, we show that the charging properties of the graphene dot are in agreement with the Coulomb blockade theory when the Fermi energy is far from the neutrality point. Thereafter, we show in Sec. IV that close to the neutrality point charging effects are strongly modified by the presence of midgap states, associated with the edges.[20] We show that electrons occupying these midgap states form a strongly correlated state, which is characterized in detail. In Sec. V, we then discuss implications for transport properties. We close with conclusions and outlook.

II. MODEL

The linearized tight-binding Hamiltonian for a graphene sheet with circular symmetry is given by

$$H_s = \hbar v_F \begin{pmatrix} 0 & e^{is\theta}\left(-is\partial_r + \frac{1}{r}\partial_\theta\right) \\ e^{-is\theta}\left(-is\partial_r - \frac{1}{r}\partial_\theta\right) & 0 \end{pmatrix}, \tag{1}$$

where $s=\pm$ determines the valley. We assume that the dot is ballistic, i.e., with no internal disorder. The general solutions with energy $\epsilon_k = \pm v_F k$ are of the type

$$\begin{pmatrix} \Psi_s^A(r,\theta) \\ \Psi_s^B(r,\theta) \end{pmatrix} = \begin{pmatrix} J_m(kr)e^{ims\theta} \\ \mp iJ_{m-s}(kr)e^{i(m-s)\theta} \end{pmatrix}, \tag{2}$$

with $J_m(x)$ denoting the mth Bessel function. The dot has a circular shape with radius R. The circular symmetry of the

 ©2008 The American Physical Society

dot allows us to classify the solutions according to their angular momenta.

In order to analyze the possible role of surface states, we assume that the boundary conditions at the edges are those appropriate for a zigzag graphene edge ending always on the same lattice site,[20]

$$\Psi_s^A(R,\theta)=0. \tag{3}$$

The boundary condition is not experimentally realizable for a circular dot, though it enables a detailed analysis of the interplay between Coulomb interaction and surface states. For the chosen boundary condition, the wave vector is quantized by $k=z_{nm}/R$, where z_{nm} denotes the nth root of the mth Bessel function, $J_m(z_{nm})=0$. In addition to the finite energy states given in Eq. (2), the boundary condition allows for surface states, which can be written as

$$\begin{pmatrix}\Psi_s^A(r,\theta)\\ \Psi_s^B(r,\theta)\end{pmatrix}=\begin{pmatrix}0\\ \sqrt{\frac{m+1}{\pi R^{2(m+1)}}}r^m e^{ism\theta}\end{pmatrix}, \tag{4}$$

with $m\geqslant 0$ to guarantee normalizability. Note that for the surface states, the angular momentum is given by sm [see Eq. (4)] and that these functions have an analytical dependence on either $z=x+iy$ or $\bar{z}=x-iy$. Discrete lattice effects impose a maximal (absolute) value on the angular momentum of order $m_{\max}\sim R/a$, where R is the radius of the disk and a is a length comparable to the lattice spacing.

Charging effects arise from electron-electron interaction, which is generally described by

$$H_C=\frac{e^2}{4\pi\epsilon_0\epsilon}\sum_{n<n'}\frac{1}{|\boldsymbol{r}_n-\boldsymbol{r}_{n'}|}. \tag{5}$$

The total Hamiltonian is given by the sum of Eqs. (1) and (5). We note that both parts scale as $1/R$. Furthermore, in graphene, $(e^2/4\pi\epsilon_0\epsilon)/\hbar v_F\approx 1$, so that both single particle and interaction energies can be expressed in units of $(e^2/4\pi\epsilon_0\epsilon R)=\hbar v_F/R$, as will be done throughout this paper.

Charging effects are mostly determined by the overall geometry of the dot, so that the lack of disorder in the model described here does not change qualitatively the main features of the Coulomb blockade. Graphene dots have, most likely, rough edges. Hence, the possible surface states are confined to certain regions of the edges. The model overestimates the number of surface states of a given dot. On the other hand, wave functions localized in the angular coordinate θ can be built from the wave functions in Eq. (2) or (4). A dot where the edge has a region of size l of the zigzag type has states localized at the edge with an angular width $\Delta\theta\sim l/R$. These states will be approximately described by superpositions of states with angular momenta $m\lesssim R/l$. Hence, when $R/l\gg 1$ and $l/a\gg 1$, these states, which will change over distances larger than the lattice spacing, will be well described by superpositions of the states derived from our continuum model.

III. CHARGING EFFECTS AWAY FROM THE DIRAC ENERGY

We analyze the effects induced by increasing the number of electrons in the dot using the Hartree approximation. The self-consistent Hartree potential describes, within a mean field approximation, the screening of charges within the dot. We assume that a half filled dot is neutral, as the ionic charge compensates the electronic charge in the filled valence band. Away from half filling, the dot is charged. Then, an electrostatic potential is induced in its interior, and there is an inhomogeneous distribution of charge.[21] We describe charged dots by fixing the chemical potential and by obtaining a self-consistent solution where all electronic states with lower energies are filled. The Hartree approximation should give a reasonable description when Coulomb blockade effects can be described as a rigid shift of the electrostatic potential within the dot.[22,23]

The Hartree potential needs to be calculated self-consistently, which must be done numerically, despite the simplicity of the model. The Dirac equation for each angular momentum channel is discretized, and an effective tight-binding model is defined for each channel. Details are given in Appendix A.

The conservation of the angular momentum allows for the possibility of solving dots with a large number of electrons. Typical results for dots charged with electrons or holes away from the Dirac energy are shown in Fig. 1. The calculation has been done in a discrete lattice with $N=100$ sites (see the Appendix). The Hartree potential changes little within the dot and, to a first approximation, the deviation from neutrality of the dot can be approximated by a rigid shift of the electrostatic potential.[21]

IV. CHARGING EFFECTS NEAR THE NEUTRALITY POINT

The Hartree calculations mentioned above fail to give a self-consistent solution when the surface band is partially occupied, and a more advanced treatment of the interaction has to be applied. This also implies that deviations from the conventional Coulomb blockade can be expected in this regime.

Instead of treating the interactions within a mean field approach, we therefore employ the method of configuration interaction to fully take into account all correlations within the truncated Hilbert space of surface states. The truncation of the Hilbert space can be justified by the energy gap to extended states of finite energy, which in our model is given by $2.4\hbar v_F/R$. In principle, the effect of the extended states can be added to the following analysis as a perturbation, but we do not expect qualitative changes of our main conclusions.

In the following we deal, therefore, with a few-electron problem and consider the eigenspectrum of N interacting electrons occupying surface states. The interaction is described in Eq. (5). Since the screening of electron-electron interaction is known to be poor close to half filling, it seems sensible to consider a long-ranged interaction rather than a (pointlike) Hubbard interaction. In addition to the particle

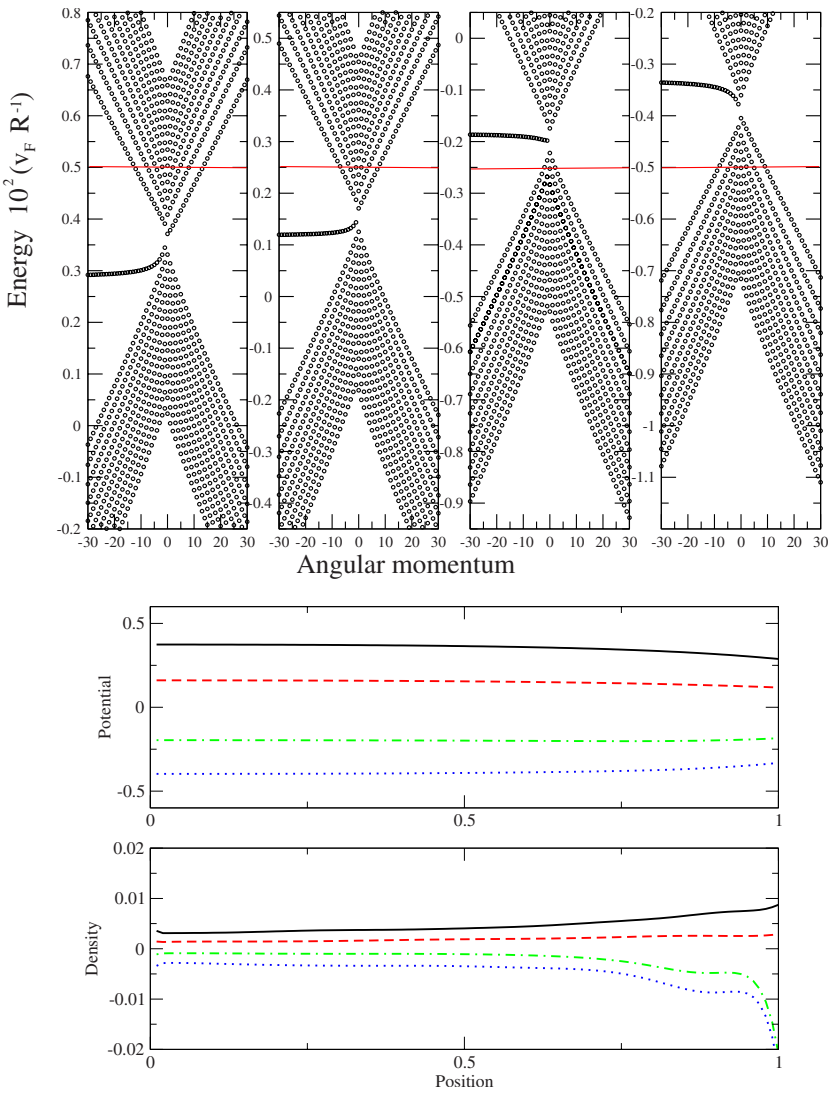

FIG. 1. (Color online) Electronic structure of a quantum dot in the Hartree approximation. All energies are in units of $\hbar v_F N/R$ with $N=100$ and the position in units of r/R. Top part: Electron energies as a function of the angular momentum, for one valley in the Brillouin zone, and different values of the chemical potential. Left: $\epsilon_F=0.5$. Center left: $\epsilon_F=0.25$. Center right: $\epsilon_F=-0.25$. Right: $\epsilon_F=-0.5$. The total number of states per valley is 12 200. The number of occupied states per valley is 6155 (left), 6122 (center left), 6066 (center right), and 6038 (right). Bottom part: Hartree potential (top), and charge density (bottom) for the four values of the chemical potential considered in the top part: Black (solid line), $\epsilon_F=0.5$. Red (dashed line), $\epsilon_F=0.25$. Green (dash-dotted line), $\epsilon_F=-0.25$. Blue (dotted line), $\epsilon_F=-0.5$.

number, the few-electron wave function can be characterized by the valley polarization $I_z=\Sigma_n s_n$ (in the absence of intervalley scattering), by the total angular momentum $M=\Sigma_n s_n m_n$, as well as by the quantum number S^2, S_z for the total spin. In the following, we limit ourselves to valley and spin-polarized solutions. While spin-polarized electrons cannot interact with each other via a pointlike Hubbard interaction (due to the Pauli principle), the long-ranged Coulomb interaction will give rise to highly correlated spin-polarized states, as shown in the rest of the paper.

Electron-electron interaction tries to maximize the distance between the electrons, which leads to a correlated ground state. The few-electron ground state for $M\to\infty$ is given by a classical Wigner crystal, where the N electrons are localized at $r=R$ and $\theta_n=2\pi n/N$, thus minimizing the Coulomb energy (see insets in Fig. 2). It is important to note that due to the localization, the truncation of the Hilbert space to include only surface states is still (in fact, even better) justified in the presence of electron-electron interactions.

Surface states are characterized by only populating one of the two sublattices and thus avoiding the kinetic energy due to nearest-neighbor hopping t. However, next-nearest-neighbor hopping $t'\approx t/10\approx 0.3$ eV connects sites within the same sublattice so that surface states gain some finite kinetic energy and the zero energy band becomes dispersive. This kinetic term delocalizes the wave function of the surface states and leads to a stable few-electron ground state with finite angular momentum M_0. From Ref. 24, the kinetic energy due to next-nearest-neighbor hopping reads $t'a^2p^2$, with a the lattice spacing and p the momentum operator. As shown in Appendix B, the Hamiltonian for next-nearest-neighbor hopping H_{kin} can be written to lowest order perturbation in t' as

$$H_{kin}=\frac{\hbar v_F}{R}\frac{3a}{10R}\sum_m m(m+1)c_m^\dagger c_m.$$

This kinetic term competes with the Coulomb interaction since it reduces the Coulomb correlations of the ground state. This competition is also visible in the dependence of the few-electron energy on the total angular momentum, as shown in Fig. 2. In the absence of next-nearest-neighbor hopping (solid line), the energy decreases with increasing angular momentum (except for oscillations discussed below) since states of higher angular momentum have lower Coulomb energy. However, when next-nearest-neighbor hopping

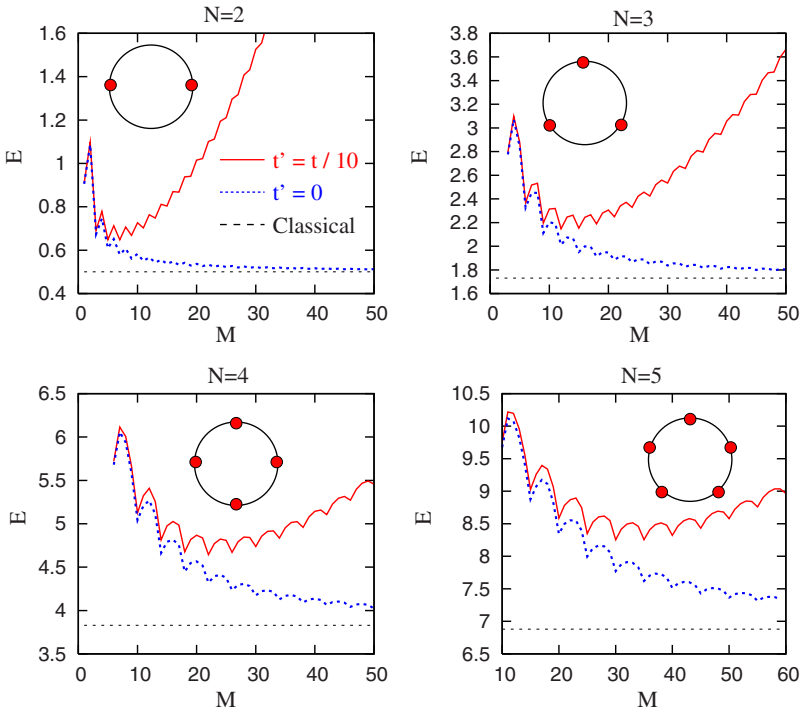

FIG. 2. (Color online) Ground-state energy (in units of $\frac{e^2}{4\pi\epsilon_0\epsilon}\frac{1}{R}$) for $N=2,3,4,5$ electrons occupying surface states as a function of the total angular momentum M with (red solid line) and without (blue dotted line) next-nearest-neighbor hopping t' (assuming $R=22$ nm). For $t'=0$ and $M\to\infty$, the energy approaches the classical energy of N point charges on a disk. The classical configuration is shown in the inset, and the classical energy is indicated by the constant dashed line.

is included, then the occupation of states with large angular momentum is hindered and the energy as function of angular momentum shows a well defined minimum. We note that the ratio between kinetic energy and Coulomb energy increases with decreasing dot size (the numerical calculations are done for $R=22$ nm). Consequently, for smaller dots, the angular momentum of the ground state decreases. In the studied subspace of valley- and spin-polarized electrons, the minimal angular momentum is given by $M_{\min}=N(N-1)/2$.

A. Trial functions for the correlated ground state

The lack of well converged Hartree solutions, which are given by Slater determinants, implies that the wave function that describes the surface states in the presence of charging effects is strongly correlated. We have chosen two Ansätze, which are compared to the numerically exact solution.

1. Laughlin wave function

The appearance of a partially filled degenerate energy band separated by an energy gap from the rest of the spectrum strongly resembles fractional quantum Hall physics. However, now, the zero energy band is caused by the boundary condition and the gap is due to the confinement rather than due to high magnetic fields. Not only the band structure is similar in both systems, but also the form of the one-particle states. Both the surface states as well as the orbitals of the lowest Landau level (in symmetric gauge) depend on z^m.

This analogy can be used to propose a trial wave function much like Laughlin's original wave function for the ground state in the fractional quantum Hall regime[25]

$$\psi(z_1,z_2,\ldots,z_N)=\mathcal{C}\prod_{i<j}(z_i-z_j)^p, \tag{6}$$

with p odd to ensure antisymmetry and $\mathcal{C}$ a normalization constant. These wave functions have a well defined total angular momentum, $M=pN(N-1)/2$. For $p=1$, this is the minimal possible angular momentum of N fully polarized electrons occupying surface states, and the trial wave function (which in this case is given by a single Slater determinant) is the exact eigenstate. With increasing value of $p=1,3,5,\ldots$, the correlations increase and the wave function is given by an increasing number of superposed Slater determinants, much like Laughlin's original wave function for the fractional quantum Hall state.[25] The Laughlin-like wave function in Eq. (6) is a parameter-free trial wave function that conserves the present symmetries (i.e., total angular momentum) and that can be uniquely expressed in the subspace of surface states. Furthermore, the factors $(z_i-z_j)^p$ create extended holes around each electron, which minimizes the Coulomb energy and explains the good agreement between the trial wave function and the numerically calculated ground state. We note, however, that we use the similarity between the studied system and the fractional quantum Hall effect only to get a trial function for the ground state, while we do not analyze the similarities between both systems in the excitation spectrum.

2. Wigner crystal

An obvious alternative to the fractional quantum Hall effect like wave function described above is that of a Wigner crystal. The surface states are maximal at the border of the dot, and the system resembles a one-dimensional system. In order to minimize the Coulomb energy, it is therefore favorable to superpose the wave functions in such a way that electrons are maximally separated in angle. We write such a trial function as

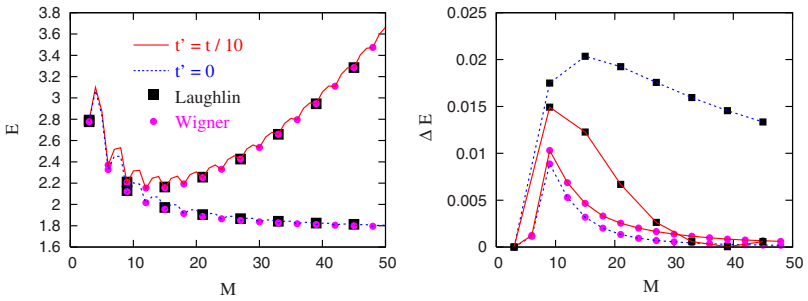

FIG. 3. (Color online) Ground-state energy for $N=3$ electrons with (full) and without (dotted) next-nearest-neighbor hopping t' in comparison with the one obtained from the trial functions. The right hand side shows energy differences. Energies are in units of $\frac{e^2}{4\pi\epsilon_0\epsilon}\frac{1}{R}$.

$$|\Psi_{WC}\rangle \equiv \sum_{\substack{m_1,m_2,\ldots,m_N \\ m_1+m_2+\cdots+m_N=M}} \left[\exp\left(-i\sum_n \frac{2\pi n m_n}{N}\right) \times \prod_{m_n} (m_n+1)^w c_{m_n}^\dagger |0\rangle\right], \tag{7}$$

where the operator $c_{m_n}^\dagger$ creates a state with momentum m_n. Note that due to the constraint imposed by the antisymmetry requirement, the wave function can only be defined for total angular momenta of the form $M=N(N-1)/2+jN$, where j is a positive integer. While the phase factor guarantees for the angular correlations in the wave function, we use the factor $(m_n+1)^w$ to optimize radial correlations (note that the normalization constant of a surface state is proportional to $\sqrt{m+1}$). For a strictly one-dimensional system, the usual definition of a quasiclassical Wigner crystal implies that $w=0$. In the numerical calculations, we choose w such that the wave function optimizes the ground-state energy ($w\approx 2$ for low M and t').

B. Correlations

For $M\to\infty$ and without next-nearest-neighbor hopping, the quantum mechanical configuration approaches the classical one, which minimizes the Coulomb energy by pinning the electrons at $r=R$ and $\varphi_n=2\pi n/N$. However, due to the rotational symmetry of our problem, the ground state is a superposition of all orientations such that there is a constant density distribution around the circumference. To characterize a Wigner crystal or, more generally, a density correlated system, one thus has to look at the density-density correlation function

$$C_M^N(\boldsymbol{r}_0,\boldsymbol{r}) = \langle N,M;0|\frac{\sum_{i\neq j}\delta(\boldsymbol{r}_0-\boldsymbol{r}_i)\delta(\boldsymbol{r}-\boldsymbol{r}_j)}{N(N-1)}|N,M;0\rangle, \tag{8}$$

where $|N,M;0\rangle$ is the ground state of the N particle system to fixed angular momentum M and $i,j\in 1,\ldots,N$.

C. Effect of disorder

We can use the same truncated basis to study disorder due to the roughness of the edges. Due to the flat dispersion in the absence of disorder, single particle states tend to localize near imperfections of the edge; however, one can show that the degeneracy of the zero energy states is only reduced by the number of impurities, which can be assumed to be much smaller than the number of surface states. The correlated state found in the presence of interactions will also be pinned by disorder, leading to glassy features.[26]

D. Numerical results

Figure 2 shows the energy of the lowest lying spin- and valley-polarized eigenstate of each total angular momentum M for $N=2,3,4,5$ electrons occupying surface states. The energies are obtained by numerically diagonalizing the few-particle Hamiltonian in this subspace. The dotted line in Fig. 2 shows the results if next-nearest-neighbor interaction is neglected, so that the total Hamiltonian consists of the Coulomb interaction only. We note two main features in that case. First, the energy oscillates as a function of the angular momentum with local minima at $M=M_{\min}(N)+jN$, where $M_{\min}(N)=N(N-1)/2$ denotes the minimal angular momentum of N-spin- and valley-polarized electrons and j is a positive integer. Only at these angular momenta can the angular correlations between the electrons be fully developed. This can be seen in the correlation functions discussed below and in the fact that only for these distinct angular momenta can a Wigner trial function be constructed. The second feature visible in Fig. 2 is that the energy generally decreases with increasing angular momentum for $t'=0$, and it finally reaches the classical limit corresponding to N point charges on the dot. The classical configurations are shown in the insets, and their energies are indicated by the constant dashed lines.

For finite t' (see solid line in Fig. 2), the Hamiltonian is supplemented by a kinetic term given in Eq. (6), which competes with the Coulomb interaction. Since the kinetic energy of surface states increases quadratically with their angular momentum, the cost in kinetic energy exceeds for large total angular momenta the gain in Coulomb energy connected with an increase in angular momentum. Thus, the N-electron system now has a ground state with well defined angular momentum M_0. The ratio between the kinetic term and the Coulomb energy grows for decreasing dot sizes, which also leads to a decrease in M_0.

In Fig. 3, we compare the numerically obtained energies for $N=3$ electrons with those of the two trial functions described above. The data for the Laughlin-like wave function [defined in Eq. (6)] are indicated by squares, while the data for a Wigner-crystal-like wave function [defined in Eq. (7)] are labeled by filled circles. First, we note that the energies of both trial wave functions differ by less than 1% from the numerical data. As noted above, the Wigner-crystal-like

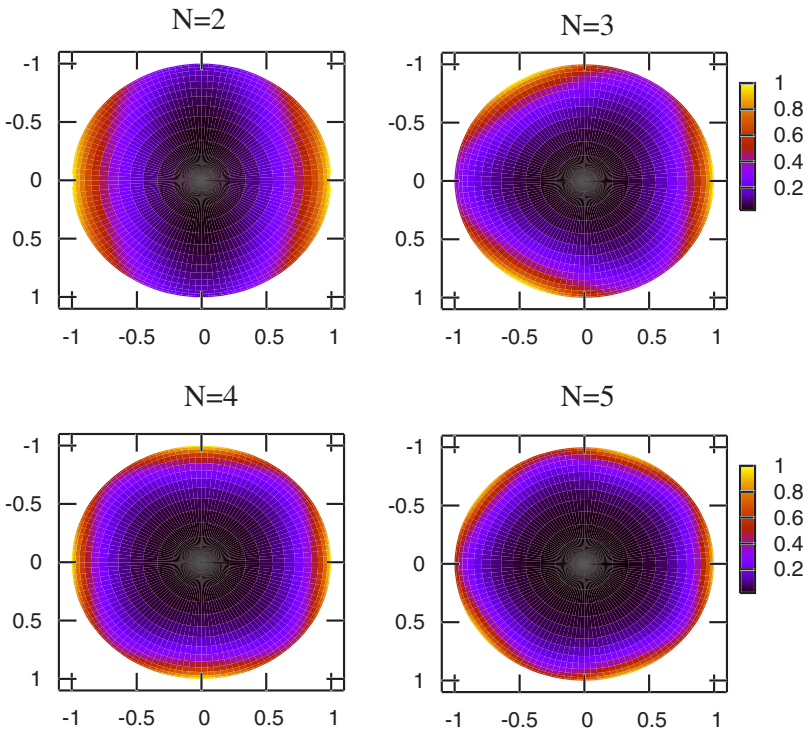

FIG. 4. (Color online) Density plot of the exact, symmetrized density-density correlation function $\tilde{C}_M^N(\boldsymbol{r})$ for $N=2,3,4,5$ particles and total angular momentum $M=N+M_{\min}$.

wave function can be constructed for each angular momentum where the few-electron energy shows a minimum. In contrast, a Laughlin-like wave function only exists for each $(N-1)$-th minimum. It is interesting to note that the Laughlin-like wave function becomes better for finite t' than for $t'=0$.

In Fig. 3, we optimized the free parameter w in the Wigner wave function for each M separately, which leads to this extremely good agreement with the exact data for both zero and finite t'. We note, however, that the optimal value was $w\approx 2$ for all M in the case of $t'=0$, while we strongly increased w with increasing M for finite t'.

Figure 4 shows the density plot of the exact, symmetrized density-density correlation function $\tilde{C}_M^N(\boldsymbol{r})=\Sigma_{i=1}^N C_M^N(R,i2\pi/N;\boldsymbol{r})$ for $N=2,3,4,5$ electrons and for $M=N+M_{\min}$. The N-fold symmetry, which is typical of a one-dimensional Wigner crystal, is clearly seen. We note that also the trail wave function shows these correlations, which explains the good agreement of its energies with the exact one.

In Fig. 5, the angular correlations along the perimeter of the dot is shown for $N=3$. An electron is fixed at $\theta=0$ and $r=R$, and the probability of finding another electron at a given angle is plotted. The left hand side of Fig. 5 illustrates that correlations are maximally developed at the distinguished angular momentum $M=jN+M_{\min}$ (here, $j=3$), while for other angular momenta the correlations are washed out. On the right hand side of Fig. 5, we see that the density-density correlations are more pronounced for higher angular momentum (here, $j=15$) while the kinetic energy t' reduces these correlations, which again is a manifestation of the competition between the Coulomb interaction and next-nearest-neighbor hopping.

V. TRANSPORT PROPERTIES

The addition of one electron to the dot, in the regime where the surface states are partially occupied, not only charges the dot and shifts the electrostatic potential, but changes the correlated wave function as well. Hence, one expects a correction to the local density of states in the dot, which is energy dependent, in a similar way to Anderson's orthogonality catastrophe[27] or the singularity in the x-ray core level photoemission.[28,29] Such Fermi edge singularities have also been discussed in relation to transport in quantum dots and nanotubes.[30–33]

The correlated state that describes the surface states of the graphene quantum dot resembles a one-dimensional system

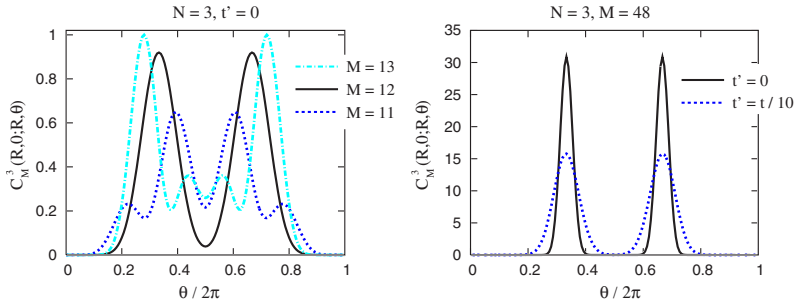

FIG. 5. (Color online) Angular correlations $C_M^N(R,0;R,\theta)$ for $N=3$ along the perimeter of the dot for various total angular momentum M (left hand side) and various next-nearest-neighbor hopping t' (right hand side).

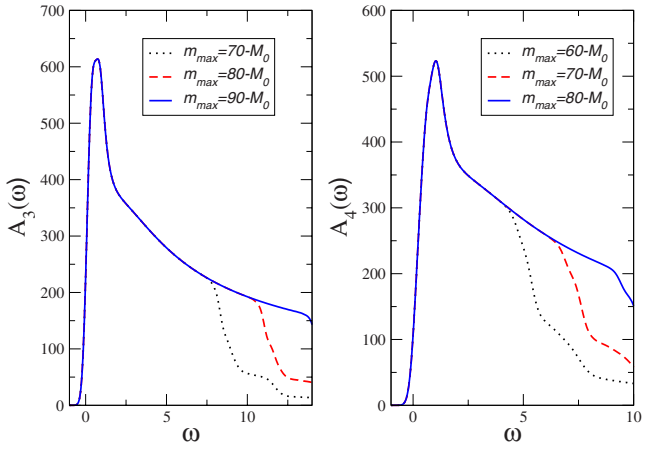

FIG. 6. (Color online) The (un-normalized) spectral function $A_N(\omega)$ for $N=3$ (left hand side) and $N=4$ (right hand side) with respect to the ground-state energies $E_0^{2,7}$ and $E_0^{3,12}$, respectively. In order to visualize the spectral density better a finite broadening of the delta peaks has been added in Eq. (9). The full, dashed, and dotted lines correspond to different maximal angular momenta.

localized along the surface. In this respect, the tunneling into this state can also be analyzed within the related framework of tunneling into correlated one-dimensional metals.[34] In this case, and in those described before, one expects that the tunneling density of states of the dot will be described by a power law. We have computed numerically the spectral function

$$A_N(\omega) \propto \sum_{M,n} \left| \langle N-1, M_0; 0 | \sum_{m=0}^{m_{\max}} c_m | N, M; n \rangle \right|^2 \times \delta(E_n^{N,M} - E_0^{N-1,M_0} - \omega), \tag{9}$$

where c_m annihilates a particle with angular momentum m. Next-nearest-neighbor hopping t' causes a finite total angular momentum M_0 of the $(N-1)$-electron ground state, and due to momentum conservation the angular momentum of the N-electron state is given by $M=M_0+m$. We restrict the m summation by an upper angular momentum.

Results for the spectral function are shown in Fig. 6, which are characterized by a sharp peak, reminiscent of the delta peak of the noninteracting system. Due to the electron-electron interaction, this peak is smeared out and decays as a power law decay, in qualitative agreement with the arguments mentioned above. There is a clear convergence for low energies as a function of the maximal angular momentum.

VI. SUMMARY AND OUTLOOK

We have presented a simple model of a graphene quantum dot, suitable for the analysis of interaction effects. We show that Coulomb blockade effects are similar to those in other systems when the chemical potential is far from the neutrality point.

The Dirac equation that describes the electronic states of graphene allows for the existence of midgap states near defects or surfaces. The presence of these states changes qualitatively the properties of the dot in the Coulomb blockade regime. As the kinetic energy of these states is nearly zero, the resulting wave function is mostly determined by the interaction and deviates significantly from a single Slater determinant. In order to describe correlations beyond mean field, we employed the method of configuration interaction within the subspace of surface states. Since it is known that screening is weak in the described case close to half filling, we considered the electrons to interact with each other via the long-ranged Coulomb interaction in contrast to a pointlike Hubbard interaction studied, for example, in Ref. 35.

Making use of the simple analytical form of the surface states, we have identified two possible correlated wave functions, which are in good agreement with few-particle exact calculations: a wave function similar to that proposed by Laughlin for the fractional quantum Hall effect and another describing a Wigner crystal. These results indicate the existence of strong correlations, although they do not allow us to analyze the existence of an incompressible electron liquid in the thermodynamic limit. We note that the correlations present in the spin-polarized states studied here arise only for long-ranged interactions, while they are absent if an effective pointlike Hubbard interaction is considered. We expect the few-particle states to be pinned by disorder at the edges (note, however, that their extension can be comparable to the dot size, so that the pinning will not be large).

The transport properties in the regime where the midgap states are partially occupied will deviate from that observed in other quantum dots. The strongly correlated nature of the wave function implies that non-shake-up effects will suppress the tunneling density of states.

An interesting extension of this work concerns the valley- and spin-degree of freedom, which will be addressed in a subsequent publication.

ACKNOWLEDGMENTS

We appreciate helpful discussions with A. H. Castro Neto, L. Brey, A. F. Morpurgo, K. S. Novoselov, and F. Sols. This work has been supported by the EU Marie Curie RTN Programme No. MRTN-CT-2003-504574, the EU Contract No. 12881 (NEST), the MEC (Spain) through Grant Nos. MAT2002-0495-C02-01, FIS2004-06490-C03-00, FIS2004-05120, and FIS2005-05478-C02-01, the Comunidad de Madrid program CITECNOMIK, and the Juan de la Cierva Programme. T. S. is supported by POCI 2010 via Project PTDC/FIS/64404/2006.

APPENDIX A: DISCRETIZATION OF THE DIRAC EQUATION

The Dirac equation for angular momentum l can be written as two coupled one-dimensional differential equations:

$$V(r)\psi_A(r) + v_F\left(i\partial_r \pm i\frac{l+1}{r}\right)\psi_B(r) = \epsilon\psi_A(r),$$

$$v_F\left(i\partial_r \mp i\frac{l}{r}\right)\psi_A(r) + V(r)\psi_B(r) = \epsilon\psi_B(r), \tag{A1}$$

where the two signs correspond to the two Dirac points. We now analyze a given Dirac equation. Extension to the other valley is straightforward. Equation (A1) can be written as

$$V(r)[\psi_A(r) + \psi_B(r)] + v_F\left(i\partial_r + \frac{i}{2r}\right)[\psi_A(r) + \psi_B(r)]$$
$$- iv_F\frac{2l+1}{2r}[\psi_A(r) - \psi_B(r)] = \epsilon[\psi_A(r) + \psi_B(r)],$$
$$V(r)[\psi_A(r) - \psi_B(r)] - v_F\left(i\partial_r + \frac{i}{2r}\right)[\psi_A(r) - \psi_B(r)]$$
$$+ iv_F\frac{2l+1}{2r}[\psi_A(r) + \psi_B(r)] = \epsilon[\psi_A(r) - \psi_B(r)]. \tag{A2}$$

We define

$$\tilde{\psi}_1(r) = \frac{\psi_A(r) + \psi_B(r)}{\sqrt{r}},$$
$$\tilde{\psi}_2(r) = \frac{\psi_A(r) - \psi_B(r)}{\sqrt{r}}, \tag{A3}$$

and we obtain

$$V(r)\tilde{\psi}_1(r) + iv_F\partial_r\tilde{\psi}_1(r) - iv_F\frac{2l+1}{2r}\tilde{\psi}_2(r) = \epsilon\tilde{\psi}_1(r),$$
$$V(r)\tilde{\psi}_2(r) - iv_F\partial_r\tilde{\psi}_2(r) + iv_F\frac{2l+1}{2r}\tilde{\psi}_1(r) = \epsilon\tilde{\psi}_2(r). \tag{A4}$$

A set of discrete equations that, taking the continuum limit, lead to Eq. (A4) is

$$\left(1 - \frac{2l+1}{4n}\right)a_n^l + \left(1 + \frac{2l+1}{4n}\right)a_{n+1}^l + v_n b_n^l = \epsilon b_n^l,$$
$$\left(1 + \frac{2l+1}{4n}\right)b_{n-1}^l - \left(1 - \frac{2l+1}{4n}\right)b_n^l + v_n a_n^l = \epsilon a_n^l. \tag{A5}$$

This set of equations is formally equivalent to a dimerized tight-binding chain, as schematically shown in Fig. 7. These chains admit zero energy estates localized at the ends when the last hopping is smaller than the previous one. In order to avoid the formation of a spurious level at the center of the dot, $n=1$, the chain is doubled, as also shown in Fig. 7. The Coulomb potential is discretized as

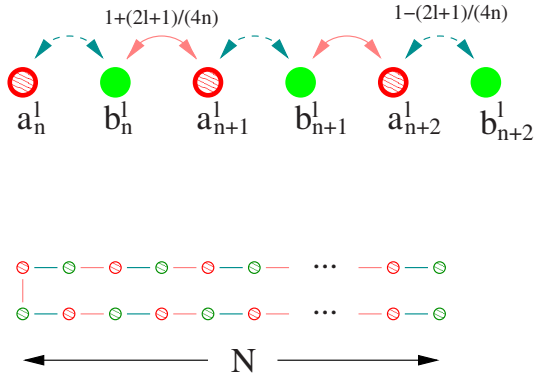

FIG. 7. (Color online) Top: Sketch of the discretization of the Dirac equation in radial coordinates used in the text. Bottom: Doubled chain used in the calculations in order to avoid spurious effects at $n=1$.

$$v_n = \sum_{m=1}^{N} v_{nm}\sum_l \frac{a_m^{l\,2} + b_m^{l\,2}}{m} \tag{A6}$$

and

$$v_{nm} = v_0\int_0^{2\pi} d\theta \frac{m}{\sqrt{m^2 + n^2 + 2mn\cos(\theta)}}. \tag{A7}$$

In terms of the original Dirac equation, the energies are expressed in units of $\hbar v_F/R$ and the parameter v_0 is given by $v_0 = (e^2/4\pi\epsilon_0\epsilon)/\hbar v_F \approx 1$.

APPENDIX B: KINETIC ENERGY DUE TO NEXT-NEAREST-NEIGHBOR HOPPING

Due to next-nearest-neighbor hopping $t' \sim 0.1t$, the initially flat band of surface states becomes dispersive. From Ref. 24, the kinetic term due to t' is given by $T = \frac{9}{4}t'a^2p^2 \to -\frac{9}{4}t'a^2\Delta$. As for the Coulomb interaction, we restrict our Hilbert space to the surface states $\psi_m(r,\theta) = \Psi^B_{s=+}(r,\theta)$ defined in Eq. (4),

$$\langle m|T|n\rangle = -\delta_{nm}\frac{9}{4}t'a^2\int d^2r\psi_m^*(\vec{r})\Delta\psi_n(\vec{r}),$$
$$\int d^2r\psi_m^*\Delta\psi_m = -\int d^2r\,\nabla\psi_m^*\nabla\psi_m + 2\pi[\psi_m^* r\partial_r\psi_m]_{r=R}.$$

In the second row, we used partial integration leading to the boundary term (second term on the right hand side). Including next-nearest-neighbor hopping, this boundary term has to vanish, while the general form of the wave function is assumed to change only close to the boundary. We thus only keep the first term, which results in

$$\langle m|T|n\rangle = \delta_{nm}\frac{9a^2t'}{2R^2}m(m+1) = \frac{\hbar v_F}{R}\frac{3a}{10R}m(m+1).$$

[1] A. K. Geim and K. S. Novoselov, Nat. Mater. **6**, 183 (2007).
[2] B. Huard, J. A. Sulpizio, N. Stander, K. Todd, B. Yang, and D. Goldhaber-Gordon, Phys. Rev. Lett. **98**, 236803 (2007).
[3] M. Y. Han, B. Özyilmaz, Y. Zhang, and P. Kim, Phys. Rev. Lett. **98**, 206805 (2007).
[4] J. R. Williams, L. DiCarlo, and C. M. Marcus, Science **317**, 638 (2007).
[5] J. B. Oostinga, H. B. Heersche, X. Liu, A. F. Morpurgo, and L. M. K. Vandersypen, arXiv:0707.2487, Nat. Mater. (to be published).
[6] F. Muñoz-Rojas, D. Jacob, J. Fernández-Rossier, and J. J. Palacios, Phys. Rev. B **74**, 195417 (2006).
[7] F. Sols, F. Guinea, and A. H. Castro Neto, Phys. Rev. Lett. **99**, 166803 (2007).
[8] J. S. Bunch, Y. Yaish, M. Brink, K. Bolotin, and P. L. McEuen, Nano Lett. **5**, 2887 (2005).
[9] M. I. Katsnelson, K. S. Novoselov, and A. K. Geim, Nat. Phys. **2**, 620 (2006).
[10] P. G. Silvestrov and K. B. Efetov, Phys. Rev. Lett. **98**, 016802 (2007).
[11] I. L. Aleiner and K. B. Efetov, Phys. Rev. Lett. **97**, 236801 (2006).
[12] T. Stauber, F. Guinea, and M. A. H. Vozmediano, Phys. Rev. B **71**, 041406(R) (2005).
[13] B. Wunsch, T. Stauber, F. Sols, and F. Guinea, New J. Phys. **8**, 318 (2006).
[14] E. H. Hwang and S. DasSarma, Phys. Rev. B **75**, 205418 (2007).
[15] S. Gangadharaiah, A. M. Farid, and E. G. Mishchenko, arXiv:0710.0622 (unpublished).
[16] A. Ghosal, A. D. Guclu, C. J. Umrigar, D. Ullmo, and H. U. Baranger, Phys. Rev. B **76**, 085341 (2007).
[17] C. Yannouleas and U. Landman, Phys. Rev. B **66**, 115315 (2002).
[18] C. Yannouleas and U. Landman, Phys. Rev. B **70**, 235319 (2004).
[19] S. M. Reimann and M. Manninen, Rev. Mod. Phys. **74**, 1283 (2002).
[20] M. Fujita, K. Wakabayashi, K. Nakada, and K. Kusakabe, J. Phys. Soc. Jpn. **65**, 1920 (1996).
[21] Note, however, that electrostatic considerations in two dimensions lead to a charge distribution, which varies smoothly over the dot, but has a $\rho(r) \propto 1/\sqrt{R-r}$ divergence at the edges.
[22] D. V. Averin and K. K. Likharev, in *Mesoscopic Phenomena in Solids*, edited by B. L. Altshuler, P. A. Lee, and R. A. Webb (Elsevier, Amsterdam, 1991).
[23] *Single Electron Tunneling*, edited by H. Grabert and M. H. Devoret (Plenum, New York, 1992).
[24] N. M. R. Peres, F. Guinea, and A. H. Castro Neto, Phys. Rev. B **73**, 125411 (2006).
[25] R. B. Laughlin, Phys. Rev. Lett. **50**, 1395 (1983).
[26] A. L. Efros and B. I. Shklovskii, J. Phys. C **8**, L49 (1975).
[27] P. W. Anderson, Phys. Rev. Lett. **18**, 1049 (1967).
[28] P. Nozières and C. T. de Dominicis, Phys. Rev. **178**, 1097 (1969).
[29] G. D. Mahan, *Many Body Physics* (Plenum, New York, 1993).
[30] M. Ueda and F. Guinea, Z. Phys. B: Condens. Matter **85**, 413 (1991).
[31] E. Bascones, C. P. Herrero, F. Guinea, and G. Schön, Phys. Rev. B **61**, 16778 (2000).
[32] D. A. Abanin and L. S. Levitov, Phys. Rev. Lett. **93**, 126802 (2004).
[33] F. Guinea, Phys. Rev. Lett. **94**, 116804 (2005).
[34] C. L. Kane and M. P. A. Fisher, Phys. Rev. Lett. **68**, 1220 (1992).
[35] J. Fernández-Rossier and J. J. Palacios, Phys. Rev. Lett. **99**, 177204 (2007).